Observations of Saturn's Ring-Plane Crossings in August and November 1995

Philip D. Nicholson, Mark R. Showalter, Luke Dones, Richard G. French, Stephen M. Larson, Jack J. Lissauer, Colleen A. McGhee, Patrick Seitzer, Bruno Sicardy, G. Edward Danielson

Observations of Saturn's ring system with the Hubble Space Telescope during the 10 August 1995 Earth crossing and the 17 to 21 November 1995 solar crossing indicate that the F ring dominates their apparent edge-on thickness of 1.2 to 1.5 kilometers. The F ring is slightly inclined with respect to the A ring, which may explain the approximately 50-minute difference in apparent crossing times for the east and west ring ansae in August. Prometheus lags its predicted position by about 19 degrees in longitude. The faint G ring is neutral or reddish in color and is confined to a radial range of 2.72 to 2.85 Saturn radii. The broad, distinctly blue E ring flares outward to a maximum thickness of about 15,000 kilometers at 7.5 Saturn radii and appears to have a spatially uniform particle size distribution.

Twice during each orbital period of 29.5 years—at alternating intervals of 13.75 and 15.75 years because of the planet's orbital eccentricity—the sun crosses Saturn's ring plane. Accompanying each solar crossing, the Earth crosses the ring plane one or three times, affording a rare opportunity to observe the vertical structure of the rings and the planet's small satellites and diffuse rings (*1*–*3*). Here we present observations with the Hubble Space Telescope (HST) during the 10 August 1995 Earth crossing and the 17 to 21 November 1995 solar crossing. Our results include ultraviolet observations of the broad, faint E ring, multicolor measurements of the tenuous G ring, and observations of discrete clumps or arcs within the narrow F ring, reminiscent of those seen in Voyager images. The spatial resolution of the HST images also allowed us to settle the issue of what determines the residual edge-on brightness of the main rings (*4*, *5*).

We used the Wide Field and Planetary Camera 2 (WFPC2) of HST during eight orbits in August and 7.5 orbits in November to determine the exact time of Earth's ring-plane crossing, measure the radial profile of edge-on ring brightness, look for ring warps, observe faint ring features, and recover the small inner satellites discovered in 1966, 1980, and May 1995 (*6*). Our observations in August were preceded by ultraviolet spectroscopic observations of the ring atmosphere (*7*). A narrowband methane filter, centered at a wavelength of 890 nm, was used for all images of the main rings and satellites to minimize scattered light from the disk of Saturn. To image the much fainter E and G rings, we used broadband filters centered at 300, 450, 555, and 675 nm. The images were processed and calibrated by standard procedures (*8*). The spatial resolution of HST is ~0.10 arc sec at 890 nm, corresponding to ~650 km at Saturn during our observations (*9*). The E and G ring images were taken in binned mode, at 0.20 arc sec (1300 km) per pixel.

Ring profiles and thicknesses. Observations of the minimum ring brightness during the Earth crossings in December 1966 (*3*) and March 1980 (*5*) yielded estimates of the rings' effective or "photometric" thickness of 2.4 ± 1.3 km and $1.1^{+0.9}_{-0.5}$ km, respectively, with the latter depending on an assumed albedo and phase function for the ring particles. It is uncertain, however, exactly what determines this effective thickness; the physical thickness, or scale height, of the rings inferred from measurements of their internal velocity dispersion is of order 10 to 50 m (*10*). Either a systematic warping of the ring plane as a result of gravitational perturbations by the sun and several Saturnian satellites (those with nonzero orbital inclinations) or local vertical (that is, out-of-plane) distortions in the form of resonantly driven bending waves within the rings were generally believed to be responsible for the observed thickness. Although theoretical calculations indicate a maximum warp of ~300 m at the outer edge of the main rings (*11*), analysis of Voyager images of bending waves driven at the strong Mimas 5:3 resonance in the A ring indicates a peak-to-peak vertical amplitude of ~1.2 km, consistent with the observed photometric thickness (*12*). Other potential contributors to the edge-on ring brightness include the narrow F ring, the "spokes" observed in Voyager images of the B ring, the tenuous but vertically extended E ring (*13*), a halo of meteoroid ejecta from the main rings (*14*), or a possible thin dust sheet extending out from the A ring (*15*).

Before the ring-plane crossing on 10 August, the radial brightness profile of the rings was quite flat and almost unvarying (Fig. 1A), but after ~21:00 UT, the brightness increased rapidly in the middle of the rings (near the B ring), tapering off outside this region. About 50 min after the ring-plane crossing, the peak brightnesses of both ansae had increased by a factor of 1.5 to 2 (Fig. 1B). There was an unexpected asymmetry in the brightnesses of the rings between east and west ansae: the central region of the west ansa was ~30% brighter than the corresponding portion of the east ansa. About an hour later, however, the two ansae were again of roughly equal brightness (Fig. 1C).

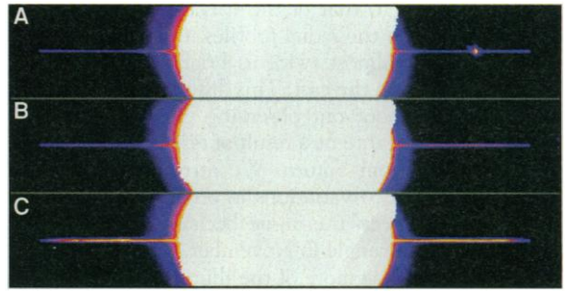

Fig. 1. A sequence of WF images at 0.89 μm obtained on 10 August 1995 as the Earth crossed Saturn's ring plane, at (**A**) 20:12, (**B**) 21:49, and (**C**) 23:42 UT. Each frame is a composite of two images, processed to remove cosmic rays and small satellites. Dione is visible 17 arc sec west of Saturn in (A). The planet's disk is heavily saturated in these 300-s exposures, and some "bleeding" is evident. North is up, and east is to the left in all figures.

P. D. Nicholson and C. A. McGhee are with the Astronomy Department, Cornell University, Ithaca, NY 14853–6801, USA. M. R. Showalter is at the Center for Radar Astronomy, Stanford University, Stanford, CA 94305, USA. L. Dones is with the San Jose State University Foundation, San Jose, CA 95172–0130, USA. R. G. French is with the Astronomy Department, Wellesley College, Wellesley, MA 02181–8286, USA. S. M. Larson is with the Lunar and Planetary Laboratory, University of Arizona, Tucson, AZ 85721, USA. J. J. Lissauer is with the Astronomy Program, Department of Earth and Space Sciences, State University of New York, Stony Brook, NY 11794–2100, USA. P. Seitzer is with the Department of Astronomy, University of Michigan, Ann Arbor, MI 48109–1090, USA. B. Sicardy is with the Observatoire de Paris, IUF/Université Paris 6, 92195 Meudon Cédex, France. G. E. Danielson is at 170-25 California Institute of Technology, Pasadena, CA 91125, USA.

Immediately before the ring-plane crossing, the vertically integrated *I/F* [reflectivity relative to a flat Lambert surface (*8*)] of the rings was essentially independent of distance from the planet, terminating abruptly at a projected radius of 140,000 ± 1000 km. This smooth appearance is in contrast with ground-based images of the dark side of the rings obtained several hours earlier (*16*), which show prominent, bright "condensations" from sunlight diffusely transmitted through the translucent C ring and Cassini division (*4*). Profiles from HST images taken at least 3.5 hours before Earth's crossing do show brightenings of 15 to 20% at the inner edge of the Cassini division and at the outer boundary of the C ring, which suggests at most a small contribution from diffusely transmitted light at this time. The average vertically integrated brightness (VIF) of the precrossing rings at a wavelength of 890 nm was 1.22 ± 0.17 km on the east ansa and 1.53 ± 0.09 km on the west ansa (*17*), consistent with measurements from 1980 (*5*).

The temporal evolution of ring brightness (Fig. 2) suggests that the east-west brightness asymmetry (Fig. 1B) reflects an earlier crossing time on the west ansa and that the subsequently reduced contrast (Fig. 1C) is caused by a steeper increase in brightness on the east ansa after the crossing. HST observations of the Earth crossing on 22 May 1995 showed no difference between east and west ansa crossing times (*18*), but a marked break in the slope of the lit-side brightness was observed on the east ansa ~1.5 hours before the actual crossing. All that can be said with certainty is that the ring-plane crossing occurred for the west ansa between 20:16 and 21:45 UT and for the east ansa between 20:33 and 21:29 UT on 10 August.

To our surprise, no change was detected in the appearance of the main rings during the 8-hour sequence of images obtained on 21 November (*1*). Sunlight diffusely transmitted through the translucent C ring and Cassini division dominates the visual appearance of the unlit rings (Fig. 3), whereas the A and B rings, effectively opaque at this low incidence angle, gleam faintly with reflected saturnshine. Outside the A ring, the narrow F ring is prominent, with a brightness comparable to that of the Cassini division (Fig. 4). In the radial profiles, the A and B rings are almost twice as bright on the west ansa as on the east. This difference persisted throughout our observing period and does not appear to be a result of residual scattered light from Saturn. We attribute part of this effect to variations in reflected saturnshine between the ansae because of the nonzero phase angle in November, with the west ansa seeing more of the illuminated globe of Saturn than did the east, although photometric modeling suggests that this effect can account for a maximum variation of only 35%.

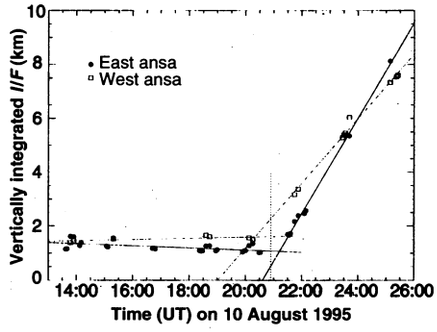

Fig. 2. The evolution of average ring brightness with time during the 10 August ring-plane crossing at a wavelength of 0.89 μm. The vertically integrated *I/F* of the rings was averaged over the radial range 80,000 to 120,000 km to improve the signal-to-noise ratio. Data from both WF and PC images are included, with each cluster of points representing a single 50-min HST observing window. Linear least-squares fits to the light curves from before and after the crossing for each ansa are shown, from which we derive crossing times of 20:20 UT ± 8 min for the west ansa and 21:09 UT ± 2 min for the east ansa. The vertical dotted line indicates the predicted crossing time of 20:54 UT (*1*).

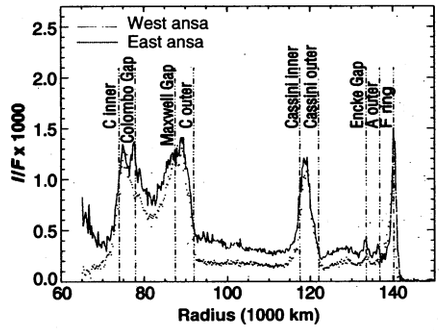

Fig. 4. Radial profiles of *I/F* derived from composites of PC images obtained during the 21 November ring-plane crossing. A simple polynomial fit to the scattered-light background has been subtracted from each composite image. East and west ansa profiles are superimposed. Prominent ring edges and gaps are identified by vertical lines. Note in particular features corresponding to the F ring (140,209 km), the outer edge of the A ring (136,780 km), the Encke gap (133,580 km), and the Colombo gap (77,750 km). Nothing is seen at the radius of the strong Mimas 5:3 bending wave (131,800 km).

In the November images, the F ring appears to be slightly inclined relative to the main rings. The F ring disappears completely about 35° beyond the west ansa. Similar behavior is not seen on the east ansa, where the ring may be traced all the way in until it is cut off by the planet's shadow (Fig. 3). The disappearance of the F ring persists throughout the 8-hour observation sequence, or over one-half of the 14.8-hour orbital period of particles in this ring, and so cannot be attributed to longitudinal structure within the ring itself. The most straightforward explanation is a shadow cast by the A ring on the F ring, which requires a relative inclination between the two rings. The latitude above the ring plane, and thus the minimum inclination, required is of order $\theta_\odot \delta a / a \sin\phi \approx 4 \times 10^{-5}$, or 0.002°, where $\theta_\odot \approx 0.001$ rad is the angular diameter of the sun at Saturn, δa = 3400 km is the radial distance between the A and F rings, a is the mean radius of the F ring, and ϕ is the longitude beyond the ansa at which the ring disappears. This value is much greater than the differential warp of the Laplace plane (*11*) between the A and F rings (2×10^{-5}°) but well below the upper limit on the F ring's inclination of 0.1° established from Voyager images (*19*). A local minimum in the F ring's brightness a few degrees beyond the west ansa also appears in the November images, again with no counterpart on the east ansa (Fig. 3). This is probably due to a combination of self-shadowing and the nonzero (5.5°) phase angle of the observations and implies that the F ring is not optically thin under conditions of edge-on solar illumination.

Both averaged images and radial profiles show subtle features in the November data, including smaller amplitude brightenings at the outer edge of the A ring—or perhaps at the nearby Keeler gap—and at the Encke gap in the outer A ring. The feature identified with the Encke gap does not corre-

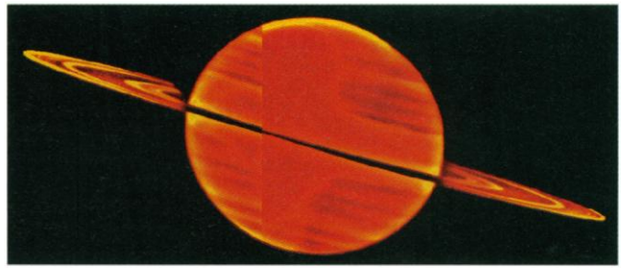

Fig. 3. A composite of images of the east (left) and west (right) ansae of Saturn's rings at 0.89 μm, acquired during the 21 November 1995 solar ring-plane crossing. Each image was constructed from an average of 10 PC frames taken over a period of 7 hours as the sun set on the visible side of the rings. The images have been high-pass filtered to remove the background light scattered from the planet and to reduce the contrast between the rings and Saturn.

spond to the nearby Mimas 5:3 bending wave. Also seen are two brightenings in the inner C ring—the outer of which is variable and may be due either to the Colombo gap or to the nearby Titan −1:0 bending wave (*20*)—as well as structure in the outer C ring. The local brightenings at the Encke gap and at the outer edge of the A ring, each of which shows a radially integrated *I/F* of 100 ± 30 m, are conceivably due to vertical edges of the ring and gap and may thus reflect the true physical thickness of the A ring (*21*).

The November images also reveal other nonaxisymmetric features in the main rings. The B ring appears brighter on the near side of the rings as a result of saturnshine, a much greater illuminated area of the planet's disk being visible from the near side of the rings. The A ring, on the other hand, shows a quadrant asymmetry reminiscent of that seen previously (*22*), with the near side brighter in the west and the far side brighter in the east. Although the sign of the asymmetry is opposite that seen in Voyager images of the sunlit side of the rings (*23*), it agrees with that predicted to be seen on the unlit side at low phase angles (*23*). Although the asymmetry seen in the A ring is consistent with that predicted by the Laplace plane warp in November, any such warp signature should persist for no more than ~30 min after sunset on the rings. As neither the A nor B ring asymmetries appeared to vary with time during our observations, we favor a model (*24*) that ascribes the asymmetry to trailing gravitational wakes in the A ring.

The August and November observations both suggest that the F ring dominates the edge-on brightness of the rings. There are several arguments in favor of the F ring's dominance. (i) In the November images, the F ring was 20 times as bright as the edge of the A ring: its average radially integrated *I/F* was ~2.0 km, compared with ~100 m for the edge of the A ring (Fig. 4). (ii) The dark-side radial profiles in August extended well beyond the outer edge of the A ring to a radius that corresponds closely to the mean radius of the F ring (*19*). This result has been confirmed by Earth-based near-infrared observations (*16, 25*). (iii) The uniformity of the August profiles and the lack of any detectable discontinuity in ring brightness either at the radius corresponding to the outer edge of the A ring or to the radius of the Mimas 5:3 bending wave argue that the A ring is obscured in edge-on viewing. (iv) The apparent asymmetry in crossing times between the east and west ansae in August and the break in slope observed in the light curve for the May ring-plane crossing (*18*) could both be caused by partial obscuration of the main rings by the inclined F ring. If the F ring is assigned an inclination and nodal orientation consistent with the November observations, its orientation can be extrapolated back to the times of the Earth crossings, using the calculated nodal regression rate of −2.70° per day. Such a calculation predicts that, at the time of ring-plane crossing on 10 August, the east ansa of the main rings was more obscured than was the west ansa, possibly causing the delay in crossing time (Fig. 2). The same model predicts symmetric obscuration and thus no east-west asymmetry on 22 May, consistent with HST observations (*18*).

Can the F ring obscure the main rings? Known amplitudes of the bending waves in the A ring (*12*) place a firm lower limit of $Z \approx 1.2$ km on the vertical thickness of whatever is concealing them. Although the vertical distribution of material within the F ring is unknown, it is possible that perturbations by Prometheus and Pandora, or moonlets within the F ring, result in an effective thickness of this order (*26*). On the other hand, the ~1-km apparent width of the F ring's dense core revealed in the Voyager radio occultation profile (*27*) implies an upper limit to its thickness in centimeter-sized particles of ~100 m. The expected brightness of the F ring may be inferred from Voyager photometry (*28*). Neglecting small color and solar phase-angle differences between the Voyager and HST data, we predict the F ring's VIF to be 0.4 to 0.8 km in the inner section of the August profiles, increasing toward a constant value of order 1 km near the ansa (*29*). This is comparable with the rings' observed edge-on VIF of 1.2 to 1.5 km (Fig. 2). Finally, although the broader component of the F ring is evidently optically thin in most or all the Voyager images (*28*), stellar (*21*) and radio (*27*) occultation profiles show that it has an opaque core about 1 km wide. A significant optical depth at low incidence or emission angles is also implied by the self-shadowing in the November HST images.

An alternative source for the edge-on brightness of the rings, consistent with the flat radial profiles, is a tenuous sheet of material between the F ring and the outer edge of the A ring, ≳1 km thick and with a normal optical depth $\tau \geq \mu_{max} \approx 1.4 \times 10^{-4}$ (here, μ is the cosine of the emission angle in August 1995). Evidence for such material has been found in Voyager images (*15*), from which a normal optical depth in the range 10^{-4} to 10^{-5} was estimated. However, an optical depth this large appears to be incompatible with the November HST images (*30*), and on this basis, we discount such a sheet as a significant contributor to the edge-on ring brightness.

Satellites and ring arcs. Ring-plane crossings provide an opportunity to observe Saturn's faint inner satellites, which are usually concealed by scattered light from the bright main rings (*31*). Janus (mean radius, $R = 89$ km) and Epimetheus ($R = 60$ km) are "horseshoe" or coorbital satellites, exchanging their positions relative to Saturn every 4 years (*32*). They have been observed once since the Voyager 2 encounter (*33*). Pandora ($R = 42$ km) and Prometheus ($R = 50$ km) orbit on either side of the F ring, apparently radially confining, or "shepherding," this narrow, complex ring.

Prometheus, Pandora, Janus, and Epimetheus are responsible for driving numerous density waves observed in the main rings, which in turn result in a significant transfer of angular momentum from the rings to the satellites (*34*). A direct measurement of the resulting secular deceleration of one or more of the satellites could provide a powerful constraint on the age of the A ring, currently suspected to be no more than $\sim 10^8$ years (*35*). Because of its mass and proximity to the rings, Prometheus is thought to be evolving most rapidly and thus offers the best opportunity for such a measurement; an accurate determination of its orbital longitude was a primary goal of our observations.

Janus, Epimetheus, and Pandora were readily identified in our August and November images at their predicted positions (*32, 36*), but Prometheus lagged behind its predicted position by ~19°, confirming HST observations from May 1995 (*37*). It was identified by its brightness, which is similar to that of Pandora, and by its orbital radius. Bosh and Rivkin (*2, 37*) also reported the discovery of a faint object, designated 1995 S1, ~25° ahead of Atlas's expected position in May 1995. This discrepancy is comparable to the expected error in Atlas's ephemeris (*36*). We have so far been unable to identify Atlas convincingly in our images, at least in part because of interference from brighter satellites or ring features. Pan does not appear to be detectable either.

Identification and measurement of the small satellites from the images required subtraction of the ring background. Pairs of consecutive frames taken with the same camera and exposure time were differenced and the resulting images examined visually for pairs of positive and negative images, displaced parallel to the ring plane (*38*). After determining centroids for all satellite images, we corrected the pixel coordinates for optical distortion in the WFPC2 (*39*) and used the positions of all visible reference satellites (usually Tethys, Dione, and Rhea) to locate the center of Saturn in each frame (*40*).

The positions of Mimas, Janus, Epimetheus, Pandora, and Prometheus relative to Saturn were fitted to eccentric, zero-inclination Keplerian orbits, with the

eccentricities fixed at previously determined values (*32, 36, 41*) and the longitudes of pericenter predicted using precession rates calculated from Saturn's zonal gravity coefficients (Table 1). The free parameters in each fit were the semimajor axis a and mean longitude at epoch λ_0; we calculated the mean angular velocity n from a using Saturn's mass and the zonal gravity coefficients J_2 and J_4 (*42*). Because of the near edge-on appearance of the orbits, we fitted the separation of each body from Saturn's center in kilometers, rather than the individual right ascension and declination offsets. For this reason, our fits are insensitive to small orbital inclinations relative to Saturn's equatorial plane. With the exception of Prometheus, the fitted orbits for the satellites agree with their previously determined orbital elements (*33, 36, 41*). Differences in the longitudes at epoch of ~1°, or 5σ to 10σ, probably reflect small errors in the Voyager mean motions and are in fact comparable to the anticipated errors after an elapsed time of 15 years.

A comparison of the fitted and predicted mean longitudes of Prometheus on 10 August and 21 November shows lags of 18.74° ± 0.10° and 18.82° ± 0.04°, respectively, similar to the 19.7° ± 0.2° measured on 22 May (*2*). If the current orbital phase lag had originated as a result of an impulsive change in Prometheus's mean motion after the Voyager 2 encounter in 1981, then we would expect the lag to be increasing by at least 0.11° per month, but its mean motion in 1995 was essentially unchanged from that in 1980 and 1981 (*43*).

We have considered a number of possible explanations for the lag in longitude. A gross error in the Voyager ephemeris appears unlikely because the other small satellites show much smaller discrepancies, and the Voyager ephemeris successfully fits seven 1966 Earth-based observations of Prometheus (*32*). The predicted lag due to the back-reaction from density-wave torques (*34*) in the 14 years since the Voyager 2 encounter is ~0.2°, ~1% of that observed. Furthermore, if the lag results from any secular effect, Prometheus's semimajor axis will equal that of the F ring only $\sim 10^4$ years in the future; this time scale seems implausibly short. A recent collision with a moonlet in the F ring has been suggested (*44*). The most recent 19-year cycle of collisions began in 1990 or later and may still be under way. Because the lag must accumulate within the last 5 years, it should have grown by at least 1° between August and November, which is inconsistent with the HST observations. A recent cometary impact is a possibility, but scaling from the impact record on Rhea (*45*), we estimate that a 0.2-km-diameter impactor strikes Prometheus once every $10^{7\pm1}$ years; the probability of such an impact in the last 14 years is $\sim 10^{-6}$.

The simplest scenario consistent with the observed lags involves a horseshoe encounter with a small coorbital satellite (*44*). In such a model, the hypothetical companion moon spends about half its time with semimajor axis $a_m = a_P + \delta a_m$ and half with $a_m = a_P - \delta a_m$, where a_P is the semimajor axis of Prometheus. The periodic changes in a_m occur near the times of closest approach between Prometheus and the moon. The 1966, 1980–1981, and 1995 data for Prometheus suggest a full libration (that is, two encounters, one raising Prometheus's orbit shortly after the Voyager encounters, the other lowering it shortly before the ring-plane crossings) with a period of ~30 years. However, this implies a rather large size for the hypothetical coorbital, comparable to that of Atlas (*46*); such an object should have been seen by Voyager (*47*).

The August HST images revealed at least 19 unidentified moving objects. Trial orbits with mean motions similar to those of Pandora or Prometheus permitted us to link most of these images with three different objects, designated 1995 S5 through S7 (*48*), on circular orbits (Table 1 and Fig. 5). These three objects are visible in all images in which they were predicted to appear before the ring-plane crossing, except when concealed by a nearby bright satellite. Their images are elongated in the plane of the rings in a manner consistent with the trailing of point sources over the durations of the exposures. On the basis of circular orbit fits, 1995 S5 and S6 lie between the orbits of Prometheus and the F ring, and 1995 S7 is at about the same distance as Prometheus. Comparing the integrated brightnesses of 1995 S5 through S7 with those of the small satellites seen in the HST images and allowing for the substantial measurement uncertainties, we derive equivalent radii of 25 ± 8 km (1995 S5) and 18 ± 5 km (1995 S6 and S7). These radii are larger than those of Pan or Atlas, and the objects should have been seen by Voyager if they are indeed moons (*47, 49*).

Although 1995 S6 and S7 remained ap-

Table 1. Satellite and ring arc orbital fits. The quoted uncertainties are formal 1σ fit errors, but partial orbit coverage means that strong parameter correlations are likely. The semimajor axis a and mean motion are calculated self-consistently, from GM_{Saturn}, J_2, and J_4 (*42*). Longitudes at epoch λ_0 and of pericenter are measured from the ascending node of Saturn's equatorial plane on the Earth's equator of J2000, at epoch 10.5 August 1995 TDT (terrestrial dynamic time) or epoch 21.5 November 1995 TDT (at Saturn). Changes in a and λ_0 are (observed − predicted) values at epoch. Values of Δa for the new objects are relative to the F ring.

Satellite	Semimajor axis (km)	Mean motion (deg/day)	Longitude at epoch	Eccentricity	Longitude of pericenter	rms residual (km)	No. of data	Δa (km)	$\Delta\lambda_0$ (deg)
			10 August 1995						
Mimas	185,414 ± 70	382.37 ± 0.19	177.11 ± 0.05	0.0201	335.7	290	21	−122	−0.47
Janus	151,317 ± 120	519.0 ± 0.6	34.92 ± 0.19	0.0066	108.0	382	7	−145	−0.33
Epimetheus	151,194 ± 40	519.62 ± 0.18	175.02 ± 0.06	0.0126	223.0	244	25	−219	0.76
Pandora	141,582 ± 130	573.6 ± 0.8	95.68 ± 0.18	0.0044	6.9	418	15	−131	−0.56
Prometheus	139,423 ± 70	587.0 ± 0.4	339.23 ± 0.10	0.0024	236.4	308	12	46	−18.74
1995 S5*	139,682 ± 370	585.4 ± 2.5	129.5 ± 0.6	0.0	–	406	17	−527	–
1995 S6*	139,742 ± 360	585.0 ± 2.6	246.0 ± 0.5	0.0	–	332	10	−467	–
1995 S7*	139,303 ± 440	587.8 ± 2.7	324.4 ± 0.6	0.0	–	443	10	−906	–
1995 S5†	139,860 ± 130	584.2 ± 0.8	129.9 ± 0.17	0.0029	14.4	417	17	−349	–
1995 S6†	139,938 ± 70	583.8 ± 0.5	246.25 ± 0.07	0.0029	14.4	316	10	−271	–
1995 S7†	139,113 ± 260	589.0 ± 1.7	324.1 ± 0.3	0.0029	14.4	402	10	−1096	–
			21 November 1995						
Mimas	185,612 ± 40	381.76 ± 0.12	282.61 ± 0.03	0.0201	78.8	131	8	76	0.06
Janus	151,742 ± 30	516.80 ± 0.16	134.02 ± 0.03	0.0066	319.0	121	8	280	0.18
Epimetheus	151,230 ± 110	519.4 ± 0.6	298.97 ± 0.11	0.0126	74.0	325	6	−183	0.94
Pandora	141,854 ± 70	572.0 ± 0.4	52.34 ± 0.06	0.0044	274.7	212	8	141	−1.17
Prometheus	139,302 ± 60	587.8 ± 0.3	349.93 ± 0.04	0.0024	160.4	142	8	−75	−18.82

*A circular orbit was fitted, but the quoted uncertainties allow for eccentricities of up to 0.003 and arbitrary pericenter longitudes. †These fits assume the F ring's eccentricity and pericenter.

proximately constant in brightness, the brightness of 1995 S5 diminished sharply as it approached either ansa of its orbit (*50*), indicating that it is extremely elongated in the direction of its orbital motion. Therefore, 1995 S5 (and likewise 1995 S6 and S7, which were never seen very near the ansa) is probably an elongated clump of debris, or arc, that is moderately opaque. Given possible systematic errors in the fitted semimajor axes, it is likely that all three objects actually orbit within the F ring (*51*), and so, we performed a second set of noncircular orbital fits (Table 1) using the F ring's eccentricity and pericenter (*52*).

We have been unable to identify 1995 S5 through S7 in the November images, but several very elongated features are visible, apparently within the F ring. The brightest of these (Fig. 6) has a full width at half-maximum (FWHM) flux of ~10°, three times that expected for a trailed point source in the F ring, and an overall length of almost 30°; it appears on the east ansa in images from three successive HST orbits. A fainter arc, with a FWHM of ~7°, is seen on the west ansa on the two previous HST orbits. Orbital fits to the indistinct leading and trailing edges of these two features yield average daily mean motions of 589° ± 6° and 584° ± 4°, respectively, consistent with either Prometheus or the F ring (*52*). Their central longitudes at epoch 21.5 November 1995 were 244° and 136°, respectively. In a composite longitudinal profile of the F ring (Fig. 7), these two bright arcs stand out clearly, along with at least four fainter clumps. This profile bears a striking resemblance to composite profiles of the F ring derived from Voyager images (*53*).

Although mean motion uncertainties preclude straightforward linking of the August and November observations, there is no correlation between the extrapolated positions of 1995 S5 through S7 and those of the arcs seen in November (Fig. 7) if we assume a mean motion equal to that of the F ring. Murray and Giuliatti Winter (*44*) have considered the possibility that 1995 S7 is the coorbital satellite responsible for Prometheus's lag. If 1995 S7 is coorbital with Prometheus, as suggested by its fitted mean motion, then it should have trailed the larger satellite by ~15° in November, but no such object is seen (Fig. 7). It is possible that the features are correlated but are located somewhere between Prometheus and the F ring, or even outside of the F ring (*54*).

The semimajor axes of 1995 S5 through S7 could be determined with much higher precision if the observations in August could be linked with one or more of the objects seen in May (*2*). Substantial uncertainties in the mean motions for all of these objects combined with the 80-day interval between observations lead to multiple potential solutions, but a systematic check of all possible linkages did yield one particularly interesting match: 1995 S3 and S6 may be linked together with a mean motion of 582.091° ± 0.002° per day, consistent with the F ring's mean motion (*52*). However, the individually fitted semimajor axes of these two objects differ by 520 ± 150 km, for an assumed eccentricity equal to that of the F ring.

The E and G rings. The broad E ring, which extends from near the orbit of Mimas to beyond the orbit of Dione, or roughly from 3 to 8 Saturn radii (R_S), was discovered during the 1966 crossing and characterized more fully in 1980 and 1981 (*55*, *56*). As inferred from its unusual blue spectrum (*57*) and a rather steep forward-scattering lobe in its phase function, this ring is composed almost entirely of 1-μm grains of water ice (*58*). Its peak normal optical depth $\tau \approx 1.5 \times 10^{-5}$.

Figure 8 shows the E and G rings as they appeared to HST on 9 August and 28 November 1995. The shape of the E ring's radial profile in August is nearly identical at all wavelengths, implying a spatially uniform particle size distribution. Even with the improved signal-to-noise ratio compared with that of previous ground-based observations, the ring is lost in the noise at $7.5R_S$ to $8R_S$. No secondary peaks in brightness are detected near the orbits of moons other than

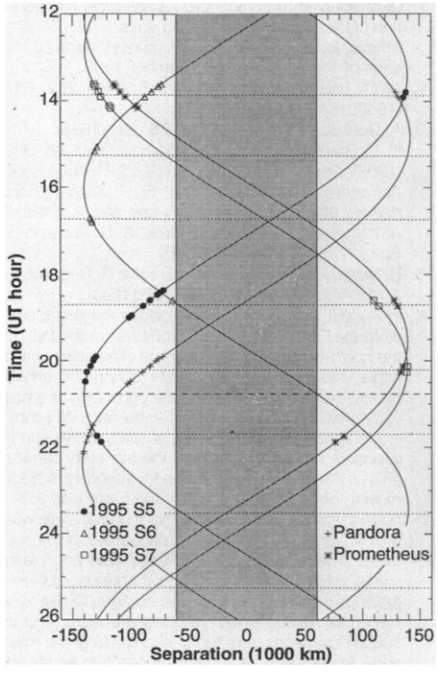

Fig. 5. Measured positions 1995 S5 (●), 1995 S6 (△), and 1995 S7 (□) on 10 August 1995, superimposed on the best-fitting circular orbits (Table 1). East is to the left. Dotted lines indicate the central time for each HST orbital window, at 96 min intervals, while the dashed line shows the predicted time of ring plane crossing; none of these faint objects was visible more than 2 hours after this time. The shaded band represents Saturn's disk. Janus, Epimetheus, and the major satellites are omitted for clarity.

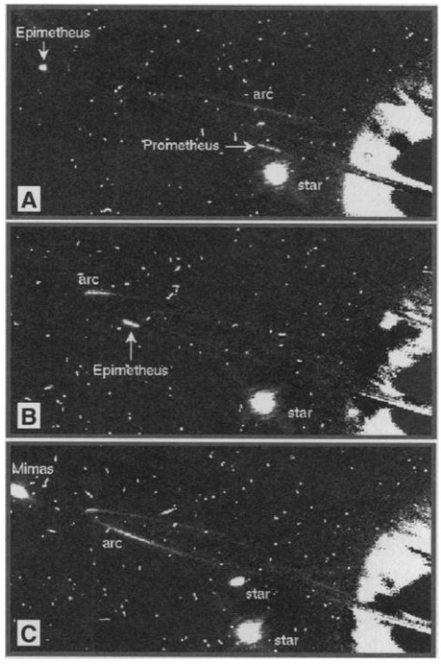

Fig. 6. Sequence of template-subtracted PC frames of the east ansa obtained on 21 November 1995 at (**A**) 13:48, (**B**) 15:24, and (**C**) 17:01 UT, showing the appearance and orbital motion of the brightest F ring arc. This ~30° long arc precedes by ~40° a fainter arc that is only clearly visible in the last frame, as it nears the ansa. Also visible are Epimetheus (near elongation in the first frame and south of the rings on the second) and Prometheus (approaching Saturn's limb in the first frame). Mimas peeks in at the edge of the last frame. The two bright objects behind and below the rings are the binary star GSC 5249-01240. The remaining streaks and speckles are due to cosmic rays.

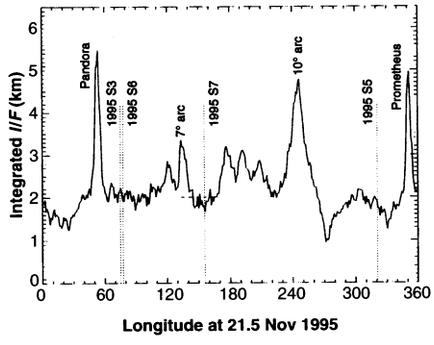

Fig. 7. Longitudinal profile of radially integrated *I/F* for the F ring, derived by combining data from 20 PC frames taken over a period of 7 hours on 21 November 1995. The two ring arcs seen most readily in the images (compare with Fig. 6) are prominent at longitudes of 244° and 136°. Pandora and Prometheus, whose motion relative to the F ring is small over 7 hours, appear as peaks at 52° and 350°. Also shown are the predicted longitudes of the objects 1995 S3 and 1995 S5 through S7.

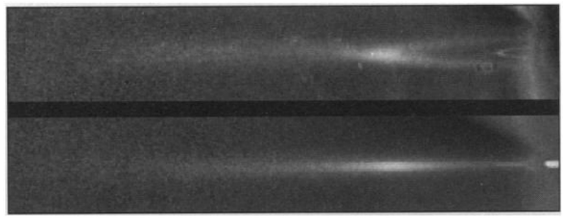

Fig. 8. Composite images of the E and G rings taken on 9 August (top) (west ansa) and 28 November (bottom) (east ansa). Each image spans a radial width of 350,000 km ($2.19R_S$ to $8.0R_S$) and a height of 60,000 km. The original WF images were recorded at a scale of 0.20 arc sec (~1300 km) per pixel. Images taken through several filters have been normalized, median-filtered, and then high-pass filtered to reduce the strong background gradient of scattered light from Saturn. The diagonal features in the lower left corners are diffraction spikes from the planet, which was just out of the field. A few residual flat-field artifacts are visible in the lower image, most noticeably just above the G ring. North is up in the top panel and down in the bottom panel.

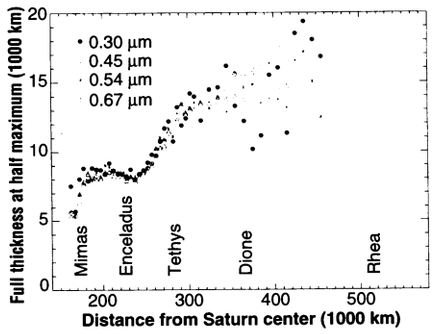

Fig. 9. The measured vertical thickness (FWHM) of the edge-on E ring as a function of distance from Saturn using data from 9 August at 0.30, 0.45, 0.54 and 0.67 μm. (Note that the projected thickness in edge-on viewing is not quite the same as local ring thickness.) The apparent thickness is a minimum of 8000 km at the radius of Enceladus, outside of which the ring flares to ~15,000 km at and beyond 6 R_S. The FWHM is independent of wavelength over the range of our data. The points at ~170,000 km are dominated by the much thinner G ring.

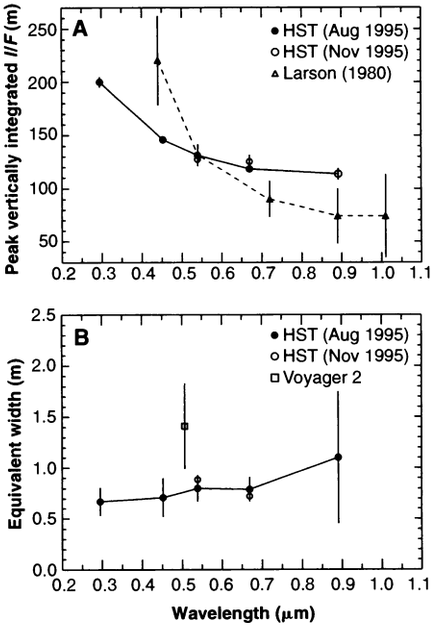

Fig. 10. (**A**) Measured peak vertically integrated brightness of the E ring in (●) August and (○) November 1995. (△) Extremely blue spectrum measured by Larson at the 1980 ring-plane crossing (*57*), scaled to the HST point at 0.55 μm. (**B**) Radially integrated brightness of the G ring in (●) August and (○) November 1995. The average level of the August data has been scaled to that of the November data to correct for contamination by the E ring in August. (□) The sole Voyager brightness measurement at low phase angle (*63*).

Enceladus, contrary to some predictions (*59*). The measured vertical FWHM in each of the four HST bandpasses shows a generally increasing thickness with radius, interrupted by a pronounced dip near the orbit of Enceladus (Fig. 9). No variation of thickness with wavelength is observable. These results are generally consistent with the conclusions of (*56*), except that our maximum measured thickness, at $\sim 7R_S$, is ~15,000 km rather than 40,000 km.

Although a pronounced blue slope is still evident in the E ring's spectrum (Fig. 10), it is less steep than the 1980 data had suggested. A comparison of the HST and Keck 2.26-μm data (*60*) shows that this slope extends well into the infrared. The somewhat flatter spectrum is more compatible with a power-law size distribution, but the sharply peaked forward-scattering phase function seen in Voyager measurements still requires a narrow size distribution. The HST spectrum is also consistent with such a distribution, if centered around a radius of 0.3 to 3 μm. The E ring's spatial distribution appears to be generally consistent with recent dynamical models (*59*, *61*), although the ring is thicker than these models predict.

The narrower and even more tenuous G ring ($\tau \approx 10^{-6}$) was discovered by Pioneer 11 (*62*) and is visible in two Voyager images (*63*), from which its radial range was determined to be 166,000 to 173,000 km. It was first seen from Earth in near-infrared images in 1995 (*60*). The Pioneer 11 signatures suggested the presence of a core of macroscopic (centimeter-size) particles capable of absorbing 100-MeV protons (*62*). The phase function derived from Voyager imaging data, on the other hand, implies a very steep size distribution, dominated by submicrometer-size particles (*63*).

The G ring appears as a short, much fainter extension of the bright rings in the August HST images (Fig. 8), terminating abruptly at a radius of 172,000 ± 2000 km ($2.85R_S$). In November, it was resolved as a ring of roughly uniform radial and azimuthal brightness, with a full radial width of 8000 ± 2000 km. The half-flux points are at 166,000 and 170,000 km, each accurate to ±1000 km, consistent with (*63*). At a scale of 1300 km per pixel, the G ring's thickness is unresolved in the August images. The ring is spectrally neutral, or perhaps slightly red (Fig. 10), suggesting that particles in this ring are somewhat larger than those found in the E ring. The measured brightness at 2.26 μm is consistent with a modest red slope (*60*) but inconsistent with the Voyager-derived phase function (*63*), which would imply a blue color.

REFERENCES AND NOTES

1. P. D. Nicholson, *Sky Telesc.* **89** (no. 5), 68 (1995); *ibid.* **90** (no. 2), 72 (1995). Predicted crossing times of 5:18 UT on 22 May 1995, 20:54 UT on 10 August 1995, 15:09 UT on 19 November 1995, and 23:34 UT on 11 February 1996 were calculated from the Saturn pole solution of (*64*) and the Jet Propulsion Laboratory planetary ephemeris DE-200. A priori uncertainties are ~1 hour for the Earth crossings and ~2 hour for the solar crossing, principally because of uncertainty in the pole's precession rate. The duration of the solar crossing was 3 days, 17 hours, and 40 min, leading to a predicted "sunset" time on the rings of 11:59 UT on 21 November 1995.
2. A. S. Bosh and A. S. Rivkin, *Science* **272**, 518 (1996).
3. A. Dollfus, *Astron. Astrophys.* **75**, 204 (1979).
4. E. E. Barnard, *Mon. Not. R. Astron. Soc.* **68**, 346 (1908); *Pop. Astron.* **30**, 547 (1922); H. N. Russell, *Astrophys. J.* **27**, 230 (1908); E. C. Slipher, *Pop. Astron.* **30**, 8 (1922); J. H. Focas and A. Dollfus, *Astron. Astrophys.* **2**, 251 (1969); A. Dollfus and S. Brunier, *Icarus* **52**, 516 (1982).
5. B. Sicardy, J. Lecacheux, P. Laques, R. Despiau, A. Auge, *Astron. Astrophys.* **108**, 296 (1982).
6. In August the sun was 1.49° above the ring plane, while the Earth was crossing from the south (dark) to the north (sunlit) side of the plane. The solar phase angle was 3.55°. On six orbits during the critical period, we obtained a sequence consisting of a pair of long-exposure (260 to 300 s) wide-field (WF) camera images showing both ring ansae and five short-exposure (100 s) images with the planetary camera (PC) of the east or west ring ansa, intended to track moving objects. In November, the Earth was 2.67° north of the ring plane, and the solar phase angle was 5.51°. Our observations were scheduled at the end of the 3.7-day period during which the ring plane swept across the sun's disk, so that we would view the rings primarily in transmitted sunlight. On each of five orbits, we obtained two long-exposure (400 to 500 s) PC images targeted to each ansa of the main rings. In both August and November, two additional orbits were dedicated to multiwavelength imaging of the E and G rings.
7. D. Hall *et al.*, *Science* **272**, 516 (1996).
8. The photometric calibration for the 890-nm images was determined from images of the DA white dwarf standard GRW+70d5824, obtained in September 1994, and was found to be the same to within 2% for PC1 and WF3 frames. This calibration was checked independently by measurements of Enceladus and Tethys, using their known geometric albedos at 550 nm and flat reflectance spectra in the red (*65*). Standard Space Telescope Science Institute (STScI) pho-

tometric calibrations were used for all images obtained with broadband filters. The incident solar flux (*66*) at Saturn, πF, integrated over the various filter passbands, was combined with the absolute flux calibration of the telescope-camera combination to yield conversion factors from raw DN (data numbers) to reflectivity of an extended source, relative to a flat Lambertian reflector: $I/F = \pi r^2 \beta DN/S_\lambda \Omega \Delta t$, where DN is the number of counts per pixel in an exposure time Δt, r is the heliocentric distance of Saturn, β is the specific flux (in ergs per second per square centimeter per angstrom) corresponding to 1 DN/s, S_λ is the solar flux at a distance of 1 astronomical unit at the wavelength of observation, and Ω is the solid angle subtended by one pixel. For the 890-nm filter, we derived $\beta = 1.918 \times 10^{-16}$ for PC1 and $\beta = 1.953 \times 10^{-16}$ for WF3, with corresponding conversion factors from DN per second to *I/F* of 0.01216 (PC1) and 0.002588 (WF3). The conversion factors derived for the broadband filters and WF camera, using values of β supplied by STScI, were 0.001389 (F300W), 6.276×10^{-5} (F450W), 2.347×10^{-5} (F555W), and 2.358×10^{-5} (F675W).
9. On 10 August, one PC1 pixel subtended 290.0 km at Saturn, and one WF3 pixel subtended 634.2 km. The corresponding values on 21 November were 304.4 and 665.7 km. Scales of 6369 and 6685 km/arc sec were used for the August and November orbital fits.
10. L. W. Esposito, M. O'Callaghan, R. A. West, *Icarus* **56**, 439 (1983); D. L. Gresh, P. A. Rosen, G. L. Tyler, J. J. Lissauer, *ibid.* **68**, 481 (1986).
11. J. A. Burns, P. Hamill, J. N. Cuzzi, R. H. Durisen, *Astron. J.* **84**, 1783 (1979).
12. F. H. Shu, J. N. Cuzzi, J. J. Lissauer, *Icarus* **53**, 185 (1983); J. J. Lissauer, *ibid.* **62**, 433 (1985).
13. A. Brahic and B. Sicardy, *Nature* **289**, 447 (1981).
14. G. E. Morfill, H. Fechtig, E. Grün, C. K. Goertz, *Icarus* **55**, 439 (1983); W. Ip, *ibid.* **115**, 295 (1995).
15. J. A. Burns, J. N. Cuzzi, M. R. Showalter, *Bull. Am. Astron. Soc.* **15**, 1013 (1983).
16. B. Sicardy *et al.*, *ibid.* **27**, 1132 (1995); *Int. Astron. Union Circ. 6269* (1995).
17. The average vertically integrated ring brightness is defined as
$$\mathrm{VIF} = (r_1 - r_2)^{-1} \int_{r_1}^{r_2} \int I/F \, dz \, dr \qquad (1)$$
where $r_1 = 80{,}000$ km and $r_2 = 120{,}000$ km. This radial range was chosen to cover the region where the ring profiles are smoothest and most consistent from image to image. The profiles inside 80,000 km are less reliable because of difficulties in removing the scattered light from Saturn. The quantity VIF is equivalent to the thickness of a solid vertical edge to the rings with a geometric albedo of unity; it is independent of any assumptions concerning the albedo or phase function of the ring particles.
18. A. S. Bosh, A. S. Rivkin, J. W. Percival, M. Taylor, W. van Citters, in preparation.
19. S. P. Synnott, R. J. Terrile, R. A. Jacobson, B. A. Smith, *Icarus* **53**, 156 (1983).
20. P. A. Rosen and J. J. Lissauer, *Science* **241**, 690 (1988).
21. A. L. Lane *et al.*, *ibid.* **215**, 537 (1982).
22. W. T. Thompson, W. M. Irvine, W. A. Baum, K. Lumme, L. W. Esposito, *Icarus* **46**, 187 (1981); L. Dones, J. N. Cuzzi, M. R. Showalter, *ibid.* **105**, 184 (1993).
23. F. A. Franklin *et al.*, *ibid.* **69**, 280 (1987).
24. G. Colombo, P. Goldreich, A. W. Harris, *Nature* **264**, 344 (1976).
25. S. M. Larson *et al.*, *Bull. Am. Astron. Soc.* **27**, 1132 (1995).
26. R. A. Kolvoord and J. A. Burns, *Icarus* **95**, 253 (1992).
27. E. A. Marouf *et al.*, *ibid.* **68**, 120 (1986).
28. M. R. Showalter, J. B. Pollack, M. E. Ockert, L. R. Doyle, J. B. Dalton, *ibid.* **100**, 394 (1992).
29. The normal equivalent width of the F ring (the radially integrated *I/F*, corrected to normal viewing geometry) measured in Voyager images at low phase angles and at 500 nm is NEW = $\mu \int I/F \, dr \approx 0.4$ km, where μ is the cosine of the emission angle (the factor of μ would be inappropriate for an optically thick ring). This quantity was approximately independent of emission angle for typical spacecraft viewing geometries (*28*). Both NEW and VIF for a narrow, optically thin ring essentially measure the total light reflected from a cross section of the ring per unit length. For an optically thin ring, we expect VIF $\leq \xi \times$ NEW/cos θ, where θ is the longitude in the ring relative to the subspacecraft longitude. The unknown factor ξ ranges between 1 and 2, depending on whether the far arm of the F ring is fully obscured or fully visible behind the F ring's near arm and the main rings. As $\theta \rightarrow 90°$, VIF approaches a maximum value of $p_{\mathrm{eff}}Z$, where p_{eff} is the ring's effective geometric albedo and Z is its physical thickness. For the F ring, whose optical depth is dominated by submicrometer ice grains, the value of p_{eff} is expected to lie in the range 0.1 to 1.
30. The region outside the A ring and interior to the F ring has an average $I/F \leq 2.2 \times 10^{-4}$. From this we estimate a normal optical depth $\tau \leq \mu(I/F)/p \approx 2 \times 10^{-5}$, where $\mu = 0.047$ in November and we have taken the geometric albedo p of the ring particles to be 0.5. The equivalent width of this sheet, EW $\leq (I/F) \times 3400$ km ≈ 0.75 km, or ~1/3 that measured for the F ring in the same images.
31. A. Dollfus, *C. R. Acad. Sci. Paris B* **264**, 822 (1967); J. W. Fountain and S. M. Larson, *Icarus* **36**, 92 (1978); S. M. Larson, B. A. Smith, J. W. Fountain, H. J. Reitsema, *ibid.* **46**, 175 (1981); P. K. Seidelmann *et al.*, *ibid.* **47**, 282 (1981); A. Dollfus and S. Brunier, *ibid.* **48**, 29 (1981); S. P. Synnott, C. F. Peters, B. A. Smith, L. A. Morabito, *Science* **212**, 191 (1981).
32. C. F. Yoder, S. P. Synnott, H. Salo, *Astron. J.* **98**, 1875 (1989).
33. P. D. Nicholson, D. P. Hamilton, K. Y. Matthews, C. F. Yoder, *Icarus* **100**, 464 (1992).
34. J. J. Lissauer, P. Goldreich, S. Tremaine, *ibid.* **64**, 425 (1985).
35. L. W. Esposito, *ibid.* **67**, 345 (1986).
36. R. A. Jacobson, *Bull. Am. Astron. Soc.* **27**, 1202 (1995).
37. A. S. Bosh and A. S. Rivkin, *Int. Astron. Union Circ. 6192* (1995).
38. In a second approach, all images with common pointing and orientation were combined with the use of median filtering to produce a template image of the rings, free of satellites and cosmic ray tracks, which could then be subtracted in turn from each of the individual images. This method was particularly useful for the November images, when the ring brightness did not change appreciably with time, and for measuring elongated objects.
39. J. Holtzman *et al.*, *Publ. Astron. Soc. Pac.* **107**, 156 (1995).
40. Satellite positions were calculated from ephemeris files maintained at the Jet Propulsion Laboratory (*36*) and implemented in the "Saturn viewer" software at the Planetary Data System's Rings Node at NASA Ames Research Center. The location of Saturn's limb was used as a pointing reference in several images for which reference moons were unavailable. In addition, the location of the edge-on ring in August was used to define the north-south location of Saturn's center. Post-fit residuals indicate that the overall accuracy of the derived satellite positions is ~400 km for the WF camera and ~200 km for the PC, or about two-thirds of a pixel. This reflects a combination of actual measurement error and ephemeris error in the reference satellites.
41. D. Harper and D. B. Taylor, *Astron. Astrophys.* **268**, 326 (1993).
42. The mean motion n is related to a by
$$n^2 = \frac{GM}{a^3}\left[1 + \frac{3}{2}J_2\left(\frac{a}{R}\right)^2 - \frac{15}{8}J_4\left(\frac{a}{R}\right)^4\right] \qquad (2)$$
where the gravitational constant G times the mass M is 3.79312×10^7 km^3/s^2, the gravitational coefficients J_2 and J_4 are 1.6297×10^{-2} and -9.10×10^{-4}, respectively, and $R = 60{,}330$ km [P. D. Nicholson and C. C. Porco, *J. Geophys. Res.* **93**, 10209 (1988)].
43. Combining the August and November fits yields an average daily mean motion of $n_{1995} = 587.2882° \pm 0.0015°$, equal to within the uncertainties to the Voyager value of $n_{\mathrm{VGR}} = 587.2890° \pm 0.0005°$ (*19*).
44. C. D. Murray and S. M. Giuliatti Winter, *Nature* **380**, 139 (1996).
45. J. J. Lissauer, S. W. Squyres, W. K. Hartmann, *J. Geophys. Res.* **93**, 776 (1988).
46. The libration period is $T_L = (4/3)Ta_P/\delta a_m$, where $T = 0.613$ days is Prometheus's orbital period; for $T_L = 30$ years, $\delta a_m = 10.4$ km. In order for Prometheus to accumulate a lag $\Delta\lambda = 19°$ in $\Delta t = 14$ years in this model, it must undergo a libration in semimajor axis of amplitude $\delta a_P = (1/3)a_P\Delta\lambda/n_P\Delta t = 0.29$ km, where n_P is the mean motion. By conservation of angular momentum, the amplitude of the libration is inversely proportional to the mass of the object; thus $M_m/M_P = \delta a_P/\delta a_m = (0.29/10.4) \approx 0.03$. Assuming the moon has the same shape and albedo as Prometheus, this body would have a brightness similar to that of Atlas.
47. S. P. Synnott, *Icarus* **67**, 189 (1986).
48. P. D. Nicholson *et al.*, *Int. Astron. Union Circ. 6243* (1995).
49. B. A. Smith *et al.*, *Science* **212**, 163 (1981).
50. *Sky Telesc.* **91** (no. 3), 11 (1996).
51. A tentative detection of 1995 S5 in Earth-based images from 9 August (B. Sicardy and F. Poulet, private communication) supports a location close to the F ring. Orbit fits for 1995 S6 and S7 using Prometheus's eccentricity and pericenter gave much larger residuals.
52. R. G. French and P. D. Nicholson, unpublished fit to Voyager and stellar occultation data (1995). The adopted mean motion of 582.05° ± 0.03° per day corresponds to the F ring's fitted $a = 140{,}209 \pm 4$ km and is consistent with the less precise value of 582.27° ± 0.20° per day derived from Voyager images in (*19*).
53. M. R. Showalter, *Bull. Am. Astron. Soc.* **26**, 1150 (1994).
54. J. N. Cuzzi and J. A. Burns, *Icarus* **74**, 284 (1988).
55. W. A. Feibelman, *Nature* **214**, 793 (1967); S. M. Larson, J. W. Fountain, B. A. Smith, H. J. Reitsema, *Icarus* **47**, 288 (1981); A. Dollfus and S. Brunier, *ibid.* **49**, 194 (1982).
56. W. A. Baum *et al.*, *Icarus* **47**, 84 (1981).
57. S. M. Larson, in *Planetary Rings*, IAU Colloquium 75, CNES, Toulouse, France, A. Brahic, Ed. (International Astronomical Union, Paris, 1984).
58. M. R. Showalter, J. N. Cuzzi, S. M. Larson, *Icarus* **94**, 451 (1991).
59. D. P. Hamilton and J. A. Burns, *Science* **264**, 550 (1994).
60. I. de Pater, M. R. Showalter, J. J. Lissauer, J. R. Graham, *Icarus*, in press.
61. M. Horanyi, J. A. Burns, D. P. Hamilton, *ibid.* **97**, 248 (1992).
62. J. A. van Allen, *J. Geophys. Res.* **88**, 6911 (1983).
63. M. R. Showalter and J. N. Cuzzi, *Icarus* **103**, 124 (1993).
64. R. G. French *et al.*, *ibid.* **103**, 163 (1993).
65. D. P. Cruikshank, J. Veverka, L. A. Lebofsky, in *Saturn*, T. Gehrels and M. S. Matthews, Eds. (Univ. of Arizona Press, Tucson, AZ, 1984), pp. 640–670.
66. *World Climate Research Programme Publication Series 7* (ITD-No. 149, World Meteorological Organization, Geneva, 1986), pp. 119–126.
67. We appreciate discussions with A. Bosh, C. Murray, J. Cuzzi, and R. Jacobson. The Laplace plane calculations were done by G. Black. The HST scheduling was handled by A. Lubenow and A. Storrs. We used the support tools provided by the Planetary Data System's Rings Node both in planning image sequences and in analyzing the satellite observations taken with the NASA/ESA HST, obtained by STScI, which is operated by the Association of Universities for Research in Astronomy under NASA contract NAS5-26555. Further support was provided by NASA grants NAGW-544, NAGW-1368, NAGW-247, and RTOPS 151-01-60-12 and 151-01-60-09. P.D.N. acknowledges the hospitality of Lowell Observatory, Flagstaff, AZ, where much of this paper was written, and Queen Mary and Westfield College, London.

4 March 1996; accepted 1 April 1996